

C2D-ISR: Optimizing Attention-based Image Super-resolution from Continuous to Discrete Scales

Yuxuan Jiang¹, Chengxi Zeng¹, Siyue Teng¹, Fan Zhang¹,
Xiaoqing Zhu², Joel Sole², and David Bull¹

¹ Visual Information Laboratory, University of Bristol, Bristol, BS1 5DD, UK

¹ {yuxuan.jiang, simon.zeng, siyue.teng, fan.zhang, dave.bull}@bristol.ac.uk

² Netflix Inc., Los Gatos, CA, USA, 95032

² {xzhu, jssole}@netflix.com

Abstract

In recent years, attention mechanisms have been exploited in single image super-resolution (SISR), achieving impressive reconstruction results. However, these advancements are still limited by the reliance on simple training strategies and network architectures designed for discrete up-sampling scales, which hinder the model’s ability to effectively capture information across multiple scales. To address these limitations, we propose a novel framework, **C2D-ISR**, for optimizing attention-based image super-resolution models from both performance and complexity perspectives. Our approach is based on a two-stage training methodology and a hierarchical encoding mechanism. The new training methodology involves continuous-scale training for discrete scale models, enabling the learning of inter-scale correlations and multi-scale feature representation. In addition, we generalize the hierarchical encoding mechanism with existing attention-based network structures, which can achieve improved spatial feature fusion, cross-scale information aggregation, and more importantly, much faster inference. We have evaluated the C2D-ISR framework based on three efficient attention-based backbones, SwinIR-L, SRFormer-L and MambaIRv2-L, and demonstrated significant improvements over the other existing optimization framework, HiT, in terms of super-resolution performance (up to 0.2dB) and computational complexity reduction (up to 11%). The source code will be made publicly available at www.github.com.

1. Introduction

Image Super-Resolution (ISR) is one of the fundamental tasks in low-level computer vision that aims to reconstruct a high-resolution (HR) image from a corresponding low-resolution (LR) version. In the past decade, in-

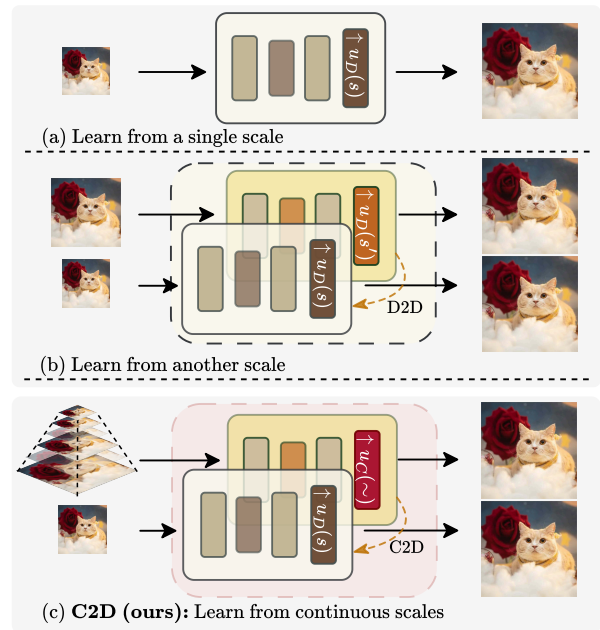


Figure 1. Different ISR training strategies: (a) the conventional training methodology [9, 16, 33] only involving training models at a fixed scale; (b) the training method based on discrete multiple scales, which can relatively improve single scale ISR performance [24, 29, 35]; (c) the proposed **C2D** training strategy, which employs a new implicit image function to learn inter-scale correlations from continuous ISR models - this strategy maintains low computational complexity and enhances the overall performance. u_C denotes the continuous up-sampler, while u_D represents the discrete up-sampler. s and s' are the up-sampling scales, and \sim stands for continuous scales.

spired by the advances in deep learning, numerous learning-based ISR methods have been developed for various applications spanning medical imaging [13, 32], satellite re-

mote sensing [52, 56], video streaming [1, 59], and surveillance [54, 60]. By leveraging data-driven feature extraction and high-capacity networks, these methods have outperformed conventional up-sampling methods based on classic signal processing theories. Among these learning-based ISR models, some [5, 8, 33, 34, 55, 66] employ attention mechanisms, e.g. Vision Transformers (ViTs), to capture global dependencies, often resulting in improved reconstruction performance compared to convolutional neural network based approaches [9, 24, 35, 63]. However, a primary concern with existing ViT-based ISR methods is the poor trade-off between performance and complexity, in particular when the application demands real-time deployment.

To mitigate the increased computational complexity associated with attention-based ISR models, various lightweight ISR models have been proposed based on different parameter reduction strategies [21, 25, 48, 57, 64]. When these methods are applied to complex ISR models, significant complexity reduction can be achieved, but only at the expense of lower reconstruction quality. Although advanced training approaches exist, such as knowledge distillation [11, 17, 22], which helps to improve lightweight model performance, these lightweight ISR models are still constrained by their limited network capacity.

In this context, inspired by the recent advances in continuous image super-resolution [6, 23, 30] and hierarchical encoding mechanisms [27, 31], this paper proposes a novel framework, **C2D-ISR**, for optimizing lightweight attention-based ISR models for discrete up-sampling scales. C2D-ISR is based on a new two-stage training strategy, which first pre-trains the target model on a continuous scale, allowing the network to fully learn the mapping between multiple scales (as shown in Figure 1). In the second stage, a more efficient and adaptable model for a single scale is then used to replace the pre-trained continuous INR up-sampler, which is fine-tuned on that fixed scale. This unique design not only inherits the detail capturing ability and multi-scale features gained from continuous-scale training, but also maintains the low complexity of the ISR model associated with the discrete-scale up-sampler. Moreover, to further trade off between performance and model complexity, we introduce a new multi-scale network design based on hierarchical encoding [27] which can more effectively extract and fuse features across different levels, thereby balancing global semantics with local details. The primary contributions of this work are summarized as follows:

- A new optimization framework is proposed for enhancing attention-based super-resolution networks. This, for the first time, enables a discrete scale ISR model to **learn from its continuous scale version**, resulting in consistently improved overall performance.
- A new hierarchical encoding based network structure,

Hierarchical Encoding Transformer (HiET) layer, has been designed to replace conventional attention-based networks. This captures information across multiple scales, resulting in reduced inference complexities and better performance. As far as we are aware, this is the **first time** that **hierarchical encoding** has been integrated with attention mechanisms for super-resolution.

- A **new U-Net architecture with adaptive window sizes** connecting different scale information has been devised to assemble HiET layers at various levels, in order to enhance multi-scale feature fusion. Unlike the traditional U-Net [45], which relies on convolution and upsampling for resolution changes, our approach adjusts the feature resolution by modifying the window size in the HiET layer at different levels. This achieves consistent performance improvements with minimal computational overhead.

We have integrated the proposed C2D-ISR framework with three efficient attention-based backbones, SwinIR-L [33], SRFormer-L [65] and MambaIRv2-L [15] and benchmarked it against HiT [62], the only comparable optimization framework in the literature. Experimental results demonstrate that C2D-ISR consistently outperforms HiT across different backbones, databases and SR tasks, resulting in optimized models with even lower complexities.

2. Related Work

Image super-resolution (ISR). Existing learning-based ISR methods are typically based on one of three popular architectures: convolutional neural networks (CNNs) [9, 24, 35, 63], vision transformers (ViTs) [5, 8, 33, 34, 55], and structured state-space models [16, 44, 46]. CNN-based models often perform feature extraction and residual learning to obtain spatial details in high-resolution content, while transformer-based models [5, 33, 38] leverage attention mechanisms to capture global dependencies, further refining SR performance. Additionally, structured state-space models build upon self-attention modules and introduce structured state-space sequences, which have been reported to outperform transformer-only architectures [15, 16]. Although these advanced network structures have achieved consistent performance improvements, the growing complexity of attention-based models also poses challenges for practical, in particular real-time, applications.

Efficient image super-resolution. To address the high complexity of attention-based ISR models, numerous lightweight architectures have been proposed that trade off efficiency and performance. Early methods focused on kernel weight reuse [25, 47] to reduce the number of parameters, but these had a limited impact on efficiency. Later approaches introduced compact architectures based on cascading residual blocks [3], information multi-distillation [3], lattice filtering [39] and structure pruning [21, 64].

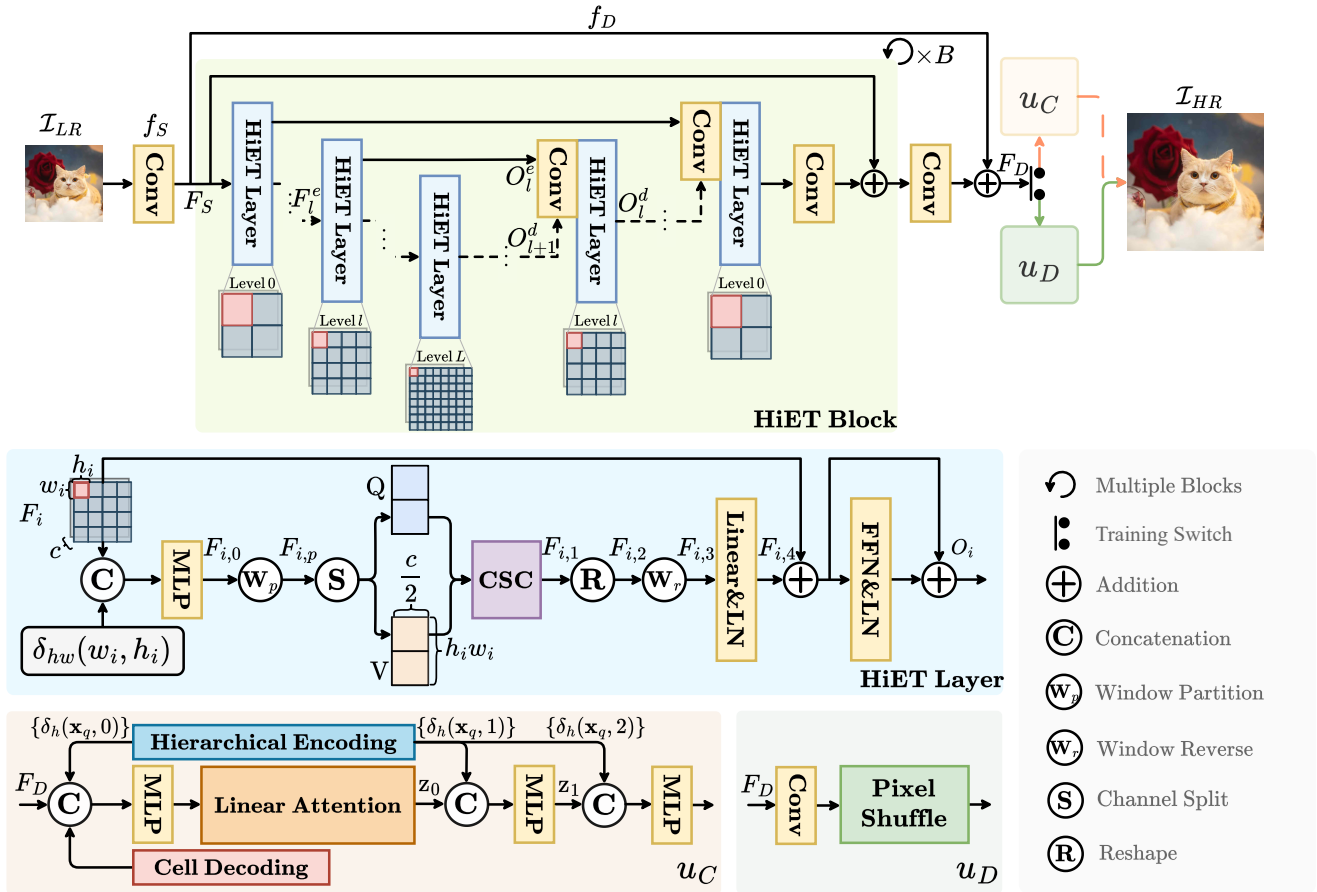


Figure 2. The architecture of the proposed C2D-ISR framework. (Top) the overall architecture and the design of the HiET block. The hyperparameter B stands for the number of HiET blocks in the deep feature extractor f_D . (Middle) the design of the HiET layer. (Bottom) the up-sampler used for continuous-scale and discrete-scale training.

More recently, lightweight network structures have been designed including SwinIR-L [33], HNCT [12], ESRT [38], ELAN [61], and Omni-SR [50]. Moreover, HiT-SR [62] proposes a spatial-channel correlation (SCC) method with linear computational complexity, while in [42], attention sharing has been proposed to alleviate the efficiency bottleneck of a self-attention layer.

Continuous super-resolution (CSR) aims to generate high-resolution (HR) images for arbitrary scaling factors, offering greater flexibility than traditional ISR methods that are typically limited to fixed up-sampling scales. Most CSR methods involve implicit image functions, which model image details continuously. Notable CSR models include MetaSR [18], LIIF [6], LTE [30] and HIIF [23], all of which can achieve improved performance compared to their corresponding discrete scale versions. However, this characteristic has not been exploited when discrete ISR models are designed and optimized.

Hierarchical encoding [27] is a new technique used in deep learning to effectively encode information at multi-

ple levels of abstraction. It enables the resulting models to progressively extract and refine features at different resolutions, enhancing feature representation and improving performance for various tasks [28, 31]. Unlike conventional single-level grid-based encoding that relies on global coordinates for position computation, hierarchical encoding leverages local coordinates to encode relative positional information. Due to the much smaller value ranges with local coordinates, the required feature grid is more compact - this can significantly reduce complexity overhead.

3. Methods

A typical attention-based image super-resolution framework consists of three key components: a shallow feature extractor, f_S , a deep feature extractor, f_D , and an up-sampler, u . Given an input low-resolution (LR) image, $\mathcal{I}_{LR} \in \mathbb{R}^{H \times W \times 3}$, the shallow feature extractor f_S employs a convolution layer to project \mathcal{I}_{LR} into a feature space $F_S = f_S(\mathcal{I}_{LR}) \in \mathbb{R}^{H \times W \times C}$, where C is the number of channels. The deep feature extractor f_D then processes F_S through a series of transformer-based blocks, followed

by another convolution layer, $F_D = f_D(F_S) \in \mathbb{R}^{H \times W \times C}$. Here, each transformer block contains multiple transformer-based layers, each of which contains a self-attention network (SA), a feedforward network (FFN), and layer normalization (LN). Finally, the up-sampler reconstructs the high-resolution (HR) image $\mathcal{I}_{HR} \in \mathbb{R}^{sH \times sW \times 3}$ from F_D , where s denotes the up-scaling factor.

In this work, our aim is to optimize the training strategy and the design of the attention network for the aforementioned framework. We first designed a two-stage training strategy, which optimizes the proposed ISR model by learning from its continuous scale counterpart while maintaining its relatively low computational complexity. To further improve the performance of the proposed model, we also designed a novel Hierarchical Encoding Transformer (HiET) layer that is integrated into HiET blocks based on a modified U-Net style architecture. This provides the backbone of the deep feature extractor f_D in this work, enhancing multi-scale information fusion and improving feature aggregation across different scales. The HiET layer leverages a hierarchical encoding mechanism to capture structural information efficiently while maintaining low computational complexity. These design details are described below.

3.1. HiET Block

Although HiT [62] adopts a variable window size mechanism to capture multi-scale information, the employed sequential arrangement only allows each layer to aggregate information from the previous one, which limits the learning of rich multi-scale features. In this work, we address this issue by incorporating a modified U-Net architecture with skip connections between paired layers and adaptive window sizes to enhance multi-scale information fusion.

Specifically, as illustrated in Figure 2. (top), each Hierarchical Encoding Transformer (HiET) block contains an encoder with $L + 1$ HiET layers and a decoder with L HiET layers. In the following description, we use superscripts e and d to differentiate their locations (in the encoder or decoder). In the encoder, the window size of the attention decreases from lower to higher layers. For each encoder layer (with index l), the input feature F_l^e is the output of the lower layer O_{l-1}^e . On the contrary, at the decoder, the window size of the attention increases at lower levels. For each decoder layer (with index l), its input F_l^d is formed by concatenating the output from the $(l + 1)$ -th decoder layer O_{l+1}^d , and that from l -th encoder layer before passing the concatenated features through a 1×1 convolution layer:

$$F_l^d = \text{Conv}([O_{l+1}^d, O_l^e]). \quad (1)$$

3.2. HiET Layer

Inspired by the hierarchical encoding mechanism proposed in [23, 27], we designed a new attention (HiET) layer,

which incorporates such hierarchical encoding with multi-scale features to better capture complex structural information and spatial dependencies. Specifically, as shown in Figure 2, in each HiET layer (within the encoder or decoder, indexed by i), given the input feature $F_i \in \mathbb{R}^{H \times W \times C}$, with window size (w_i, h_i) , the embedded hierarchical encoding δ_{hw} at feature index (u, v) is defined as:

$$\delta_{hw}(w_i, h_i) = (\lfloor \frac{u}{w_i} \times 2 \rfloor \bmod 2, \lfloor \frac{v}{h_i} \times 2 \rfloor \bmod 2), \quad (2)$$

where $u = 0, 1, \dots, W - 1$, $v = 0, 1, \dots, H - 1$. It is concatenated with the input feature F_i and passed through a multilayer perceptron (MLP), resulting in $F_{i,0}$:

$$F_{i,0} = \text{MLP}([F_i, \{\delta_{hw}(w_i, h_i)\}]), \quad (3)$$

where $\{\cdot\}$ stands for the set of all points, i.e. $\{\delta_{hw}(w_i, h_i)\} \in \mathbb{R}^{H \times W \times 2}$. $F_{i,0}$ is then partitioned into non-overlapped subblocks according to the corresponding window size (w_i, h_i) and each of them is reshaped as $F_{i,p} \in \mathbb{R}^{h_i w_i \times C}$, where subblock index is omitted for simplicity. A channel-splitting operation is performed after reshaping to obtain two sets of features, Q and V :

$$[Q, V] = \text{split}(F_{i,p}), \quad (4)$$

where $Q, V \in \mathbb{R}^{h_i w_i \times \frac{C}{2}}$. We then apply Channel Self-Correlation (CSC) [62] to leverage different window sizes and effectively utilize rich multi-scale information for performance enhancement while maintaining low complexity,

$$F_{i,1} = (\frac{Q^T V}{h_i w_i} V^T)^T. \quad (5)$$

Here $(\cdot)^T$ represents matrix transpose, and $F_{i,1} \in \mathbb{R}^{h_i w_i \times \frac{C}{2}}$. $F_{i,1}$ is then reshaped into $F_{i,2} \in \mathbb{R}^{h_i \times w_i \times \frac{C}{2}}$, and reversed to match the spatial resolution of F_i , resulting in $F_{i,3} \in \mathbb{R}^{H \times W \times \frac{C}{2}}$. To restore the channel dimension, we apply a linear transformation followed by layer normalization, resulting in $F_{i,4} \in \mathbb{R}^{H \times W \times C}$:

$$F_{i,4} = \text{LN}(\text{Linear}(F_{i,3})). \quad (6)$$

Finally, through a skip connection and feedforward network (FFN), the output of this layer is obtained, denoted as O_i .

3.3. Training Methodology: C2D

As mentioned above, all existing ISR optimization frameworks [16, 33, 61, 62, 65] adopt simple training strategies based on a fixed up-sampling factor. It is noted that continuous super-resolution methods can deal with arbitrary up-sampling ratios with a single model and exhibit improved performance over discrete ISR approaches at their pre-trained scales. However, this characteristic has not been exploited during the training of discrete ISR models. To this

end, we designed a novel two-stage training methodology to boost the training performance of our optimization framework, which consists of two stages: i) Continuous-Scale Pre-Training; ii) Discrete-Scale Fine-Tuning.

Stage 1: Continuous-Scale Pre-Training. We first optimize a continuous-scale model designed to exploit inter-scale correlations. By learning how to up-sample to arbitrary scales, the model is expected to learn the correlation between multiple scales and better recover high-frequency details. Inspired by [23], we designed a lightweight implicit image function, HIIF-L, to achieve continuous-scale up-sampling (u_C in Figure 2). HIIF-L is associated with a relatively small model size (compared to the original HIIF [23]), only consisting of three MLPs and a linear attention module. This will enable sufficient optimization of the HiET blocks rather than relying on the lightweight HIIF-L to obtain satisfactory super-resolution performance.

Specifically, the input of the first MLP is the concatenation of the deep feature F_D obtained from f_D and $cell = [\frac{2}{s_H}, \frac{2}{s_W}]$ that represents cell decoding and hierarchical coordinates, s stands for the up-sampling factor. Following [23], the hierarchical coordinate $\delta_h(\mathbf{x}_q, j)$ is derived from the local coordinate $\mathbf{x}_q = (x_{local}, y_{local})$:

$$\delta_h(\mathbf{x}_q, j) = \lfloor \mathbf{x}_q \times 2^{j+1} \rfloor \bmod 2, \quad (7)$$

where j indexes the current level of the hierarchy. Intuitively, this allows HIIF-L to handle multi-scale structures by encoding fine-grained positional information. The resulting features then undergo a linear attention mechanism that modulates global-local context:

$$\mathbf{z}_0 = \text{MHA}(\text{MLP}([F_D, \{\delta_h(\mathbf{x}_q, 0)\}, cell])), \quad (8)$$

where $\mathbf{z}_0 \in \mathbb{R}^{sH \times sW \times dim}$ denotes the feature output of the linear attention. In this work, we set dim equal to C . The refined features are then fed into the second MLP, which predicts the final high-resolution outputs $I_{HR} \in \mathbb{R}^{sH \times sW \times 3}$:

$$\mathbf{z}_1 = \text{MLP}([\mathbf{z}_0, \{\delta_h(\mathbf{x}_q, 1)\}]). \quad (9)$$

This design enables HIIF-L to seamlessly adapt to different scale factors, preserving both global structures and high-frequency details.

Stage 2: Discrete-Scale Fine-Tuning. In the second stage, we replaced HIIF-L with a commonly used sub-pixel convolution (u_D in Figure 2) and trained the resulting ISR model for three fixed scaling factors ($\times 2$, $\times 3$, and $\times 4$). We first initialize the weights of f_S and f_D with the model parameters obtained in Stage 1, and then fine-tune them alongside the discrete up-sampler (u_D). These fine-tuned weights are ultimately used for model inference at the target scales.

$$\mathcal{I}_{HR} = \text{Pixelshuffle}(\text{Conv}(F_D)). \quad (10)$$

4. Experiment Configuration

Implementation details. We adopt L1 as the loss function during the training and use the Adam [26] optimizer. In the first training stage (at the continuous scale), the maximum and minimum learning rates are set to 4×10^{-4} and 1×10^{-6} , respectively, while in the second stage (at the discrete scale), their values are 1×10^{-5} and 1×10^{-6} instead. Models are trained for 1000 epochs with a batch size of 16 in each stage: 700 epochs for the first stage and 300 epochs for the second stage. Following a 50-epoch warm-up phase, the learning rate is decayed according to a cosine annealing schedule [37]. The training and inference of all (proposed and benchmark) models were based on a single NVIDIA RTX 4090 graphics card.

Baseline models. Following [62], we applied our C2D-ISR optimization framework to three latest lightweight ISR methods, SwinIR-L [33], SRFormer-L [65] and MambaIRv2-L [15]. Compared to [62], we replaced one of the anchor models, SwinIR-NG, with a more recent model, MambaIRv2-L [15]. All C2D-ISR optimized models retain the same hyperparameter settings as their corresponding original versions. Specifically, for SwinIR-L [33] and SRFormer-L [65], we set window sizes to [64, 32, 8, 8, 32, 64] for the six layers in each block respectively; for MambaIRv2-L [15], window sizes are set to [64, 32, 8, 32, 64] for the five layers in each block. All other settings, such as the number of blocks $B = 4$, the number of channels C , and FFN design, remain unchanged as the original models. For each anchor model, we compare our approach with HiT [62], the only existing comparable method in the literature, and the pre-trained, unoptimized version. To offer additional benchmarks, we also provide results for other efficient ISR approaches, including HiT-SNG [62], SwinIR-NG [7], EDSR-B [35], CARN [3], IMDN [20], LatticeNet [39], RFDN-L [36], FMEN [10], GASSL-B [51], HNCT [12], ELAN-L [61] and Omni-SR [50] in this paper¹.

Datasets. Following the previous works [6, 35, 62], we use the DIV2K training dataset [2] from the NTIRE 2017 Challenge [49] for network optimization, which consists of 800 images in 2K resolution. In Stage 1, we utilize the training methodology described in [6, 23], and sample B_s random scaling factors $s_{1 \dots B_s}$ from a uniform distribution $\mathcal{U}(1, 4)$, i.e. in-scale, where B_s is the batch size. We also use the same scale factor for height and width, i.e. $s_x = s_y = s$, to crop $64s \times 64s$ patches from original images and generate their 64×64 down-sampled counterparts based on bicubic resizing [43]. In Stage 2, we fix the s to 2, 3 and 4 for different discrete scales, $\times 2$, $\times 3$ and $\times 4$ respectively. Data augmentation strategies, such as random rotations and horizontal flips, are also applied during model training.

¹The results of these additional benchmarks are summarized in the *Supplementary* due to the limited space, but are used to plot Figure 5.

Method	Scale	Complexity		Set5		Set14		BSD100		Urban100		Manga109	
		#Para.↓	FLOPs↓	PSNR↑	SSIM↑	PSNR	SSIM	PSNR	SSIM	PSNR	SSIM	PSNR	SSIM
SwinIR-L[33]	×2	910K	244.4G	38.14	0.9611	33.86	0.9206	32.31	0.9012	32.76	0.9340	39.12	0.9783
SwinIR-HiT[62]		772K	209.9G	38.22	0.9613	33.91	0.9213	32.35	0.9019	33.02	0.9365	39.38	0.9782
SwinIR-C2D (ours)		755K	201.2G	38.27	0.9612	33.98	0.9211	32.39	0.9020	33.14	0.9370	39.43	0.9784
SwinIR-L[33]	×3	918K	110.8G	34.62	0.9289	30.54	0.8463	29.20	0.8082	28.66	0.8624	33.98	0.9478
SwinIR-HiT[62]		780K	94.2G	34.72	0.9298	30.62	0.8474	29.27	0.8101	28.93	0.8673	34.40	0.9496
SwinIR-C2D (ours)		763K	90.6G	34.81	0.9299	30.65	0.8473	29.33	0.8099	29.04	0.8687	34.46	0.9494
SwinIR-L[33]	×4	930K	63.6G	32.44	0.8976	28.77	0.7858	27.69	0.7406	26.47	0.7980	30.92	0.9151
SwinIR-HiT[62]		792K	53.8G	32.51	0.8991	28.84	0.7873	27.73	0.7424	26.71	0.8045	31.23	0.9176
SwinIR-C2D (ours)		775K	52.7G	32.61	0.8997	28.89	0.7875	27.77	0.7426	26.87	0.8063	31.33	0.9181
SRFormer-L[65]	×2	853K	236.2G	38.23	0.9613	33.94	0.9209	32.36	0.9019	32.91	0.9353	39.28	0.9785
SRFormer-HiT[62]		847K	226.5G	38.26	0.9615	34.01	0.9214	32.37	0.9023	33.13	0.9372	39.47	0.9787
SRFormer-C2D (ours)		830K	218.4G	38.33	0.9619	34.18	0.9225	32.45	0.9028	33.28	0.9382	39.53	0.9789
SRFormer-L[65]	×3	861K	104.8G	34.67	0.9296	30.57	0.8469	29.26	0.8099	28.81	0.8655	34.19	0.9489
SRFormer-HiT[62]		855K	101.6G	34.75	0.9300	30.61	0.8475	29.29	0.8106	28.99	0.8687	34.53	0.9502
SRFormer-C2D (ours)		838K	98.3G	34.84	0.9302	30.71	0.8488	29.34	0.8108	29.17	0.8707	34.57	0.9499
SRFormer-L[65]	×4	873K	62.8G	32.51	0.8988	28.82	0.7872	27.73	0.7422	26.67	0.8032	31.17	0.9165
SRFormer-HiT[62]		866K	58.0G	32.55	0.8999	28.87	0.7880	27.75	0.7432	26.80	0.8069	31.26	0.9171
SRFormer-C2D (ours)		849K	57.0G	32.67	0.9002	28.91	0.7883	27.80	0.7439	26.96	0.8104	31.45	0.9180
MambaRv2-L[15]	×2	774K	286.3G	38.26	0.9615	34.09	0.9221	32.36	0.9019	33.26	0.9378	39.35	0.9785
MambaRv2-HiT [†] [62]		638K	164.5G	38.28	0.9615	34.11	0.9225	32.40	0.9022	33.30	0.9387	39.38	0.9788
MambaIRv2-C2D (ours)		631K	152.9G	38.31	0.9618	34.16	0.9228	32.45	0.9021	33.40	0.9396	39.43	0.9792
MambaRv2-L[15]	×3	781K	126.7G	34.71	0.9298	30.68	0.8483	29.26	0.8098	29.01	0.8689	34.41	0.9497
MambaRv2-HiT [†] [62]		645K	77.5G	34.75	0.9299	30.70	0.8480	29.27	0.8099	29.07	0.8693	34.50	0.9500
MambaIRv2-C2D (ours)		638K	69.0G	34.78	0.9303	30.78	0.8488	29.36	0.8105	29.15	0.8701	34.56	0.9503
MambaRv2-L[15]	×4	790K	75.6G	32.51	0.8992	28.84	0.7878	27.75	0.7426	26.82	0.8079	31.24	0.9182
MambaRv2-HiT [†] [62]		653K	42.0G	32.50	0.8990	28.84	0.7877	27.78	0.7427	26.84	0.8083	31.27	0.9186
MambaIRv2-C2D (ours)		647K	40.0G	32.59	0.8996	28.89	0.7883	27.86	0.7432	26.96	0.8097	31.37	0.9195

Table 1. Quantitative comparison with state-of-the-art SR methods on the Set5 [4], Set14 [58], BSD100 [40], and Urban100 [19] and Manga109 [41]. The output size is set to 720×1280 for all scales to compute FLOPs. The symbol [†] indicates that the corresponding benchmark model was implemented by us following its original literature. The best result is colored in blue.

Evaluation Metrics. Five commonly used benchmark datasets: Set5 [4], Set14 [58], BSD100 [40], Urban100 [19] and Manga109 [41], are employed for model evaluation. Here, the LR images are obtained from their HR counterparts through bicubic degradation. We conduct comparisons under three up-scaling factors: $\times 2$, $\times 3$, and $\times 4$, and assess the SR performance using PSNR and SSIM [53].

5. Results and Discussion

5.1. Overall Performance

Quantitative results. Table 1 summarizes the quantitative results, comparing the proposed C2D-ISR framework to HiT and the anchor lightweight model for three backbones, SwinIR-L [33], SRFormer-L [65] and MambaRv2-L [15], in terms of PSNR, SSIM and complexity (model sizes and FLOPs). It can be observed that the proposed C2D-ISR consistently outperforms HiT (and the lightweight versions) across all backbones, databases, quality metrics and different up-sampling tasks ($\times 2$, $\times 3$ and $\times 4$), with PSNR gains up to 0.2dB. Moreover, the resulting model complexity is

also lower in each case. This confirms the superior performance of the proposed approach. We have also showcased this by plotting the average PSNR performance of all benchmark models against their corresponding complexity figures (in terms of FLOPs), as shown in Figure 5, which confirms the excellent complexity-performance trade-off achieved by the proposed framework.

Qualitative results. Visual comparisons between the generated results by C2D-ISR optimized, HiT optimized and the lightweight backbone models are provided in Figure 3. It can be observed that C2D-ISR offers better reconstruction results compared to the benchmark methods, with fewer blocky or structural artifacts. We further utilize Local Attribution Maps (LAM) [14] to evaluate the effectiveness of information aggregation. Specifically, as illustrated in Figure 4, we apply LAM to SRFormer [65], SRFormer-HiT [62], and SRFormer-C2D for the same target regions highlighted by red boxes. The visualization results, where larger informative areas indicate stronger aggregation capability, demonstrate that our method captures a broader range of in-

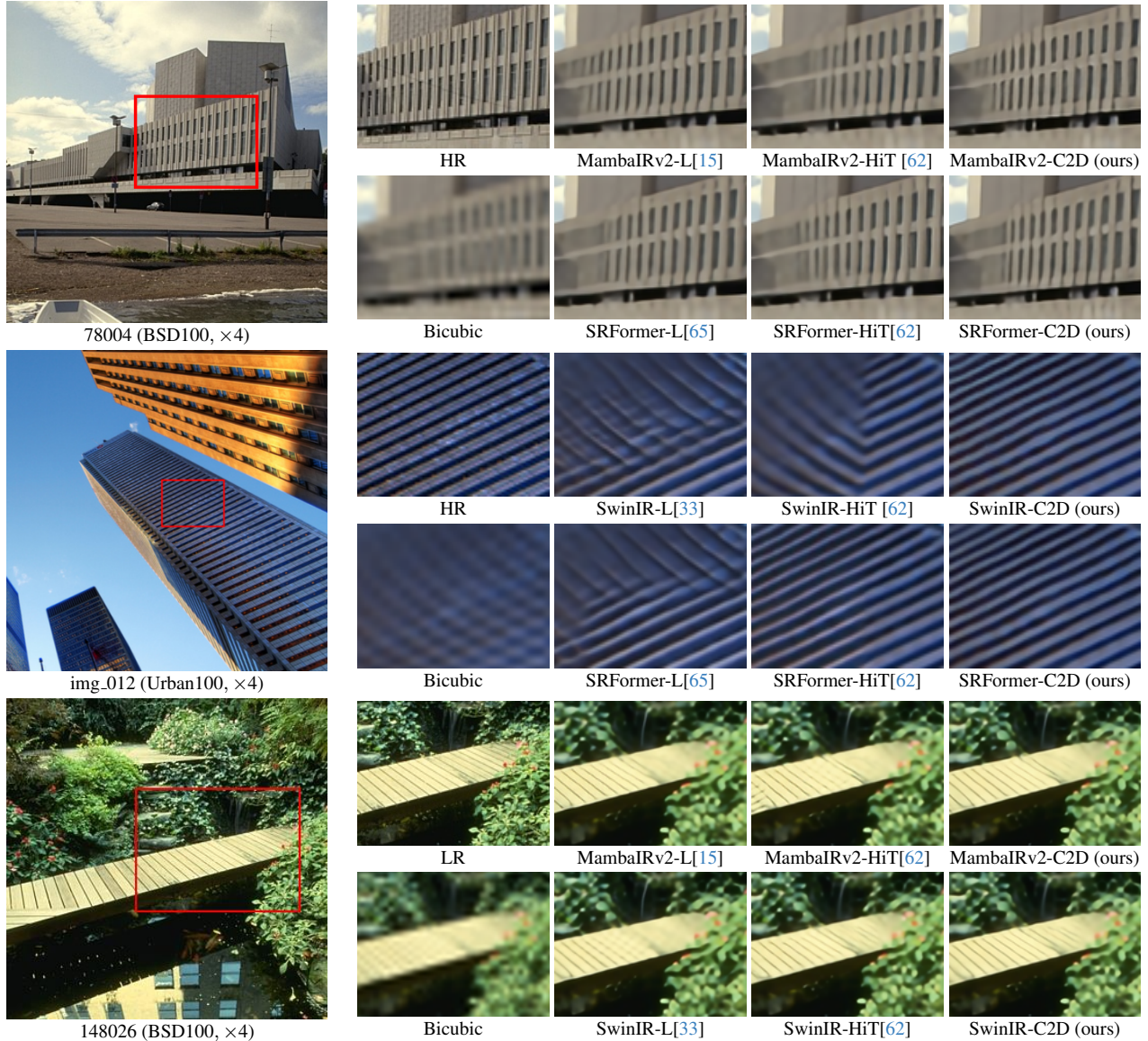


Figure 3. Qualitative comparisons between the proposed C2D-SR framework and HiT [62].

formation, which can potentially enhance SR performance.

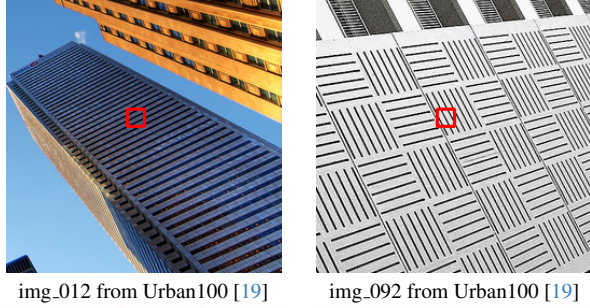
5.2. Ablation Study

We have designed an ablation experiment to verify three main contributions of this work.

C2D training strategy. To test the proposed C2D training strategy, we created the following variants: (v1.1-w/o C) without the pre-training on continuous scales; (v1.2-w/o D) without fine-tuning on the discrete scales, i.e., using HIIF-L for all ISR tasks. Based on the results in Table 2, we can confirm that learning from continuous scales plays a crucial role in improving single-scale performance, with v1.1 significantly outperformed by the full C2D model. More-

over, the continuous-scale upsampler (v1.2) exhibits much higher computational complexity, requiring approximately four times the FLOPs, compared to full C2D.

HiET layer. To verify the effect of our layer design, we modified the HiET layer to obtain: (v2.1-w/o HiE) by removing the hierarchical encoding embedded with the input feature and (v2.2-w/o CSC) by replacing the CSC module with the SCC proposed in [62]. From Table 2, we can observe that embedding hierarchical encoding (based on v2.1) does enhance reconstruction performance while introducing only minimal parameter overhead. Although utilizing the full SCC structure (v2.2) provides a minor performance improvement, it evidently increases the number of param-



img_012 from Urban100 [19]

img_092 from Urban100 [19]

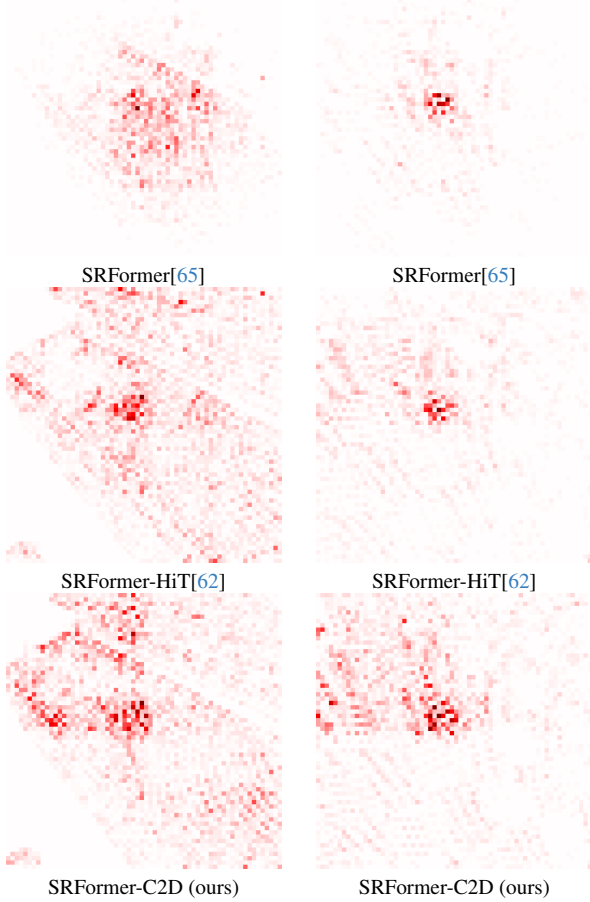


Figure 4. The illustration of the local attribution maps (LAM) comparisons by using the Local Attribution Maps tool[14].

eters and the FLOPs - this shows the better performance-complexity trade-off of the HiET layer structure.

HiET Block. To evaluate the contribution of our block design, we replaced the new U-Net architecture with the original linear structure in each backbone model (v3.1-w/o U-Net). We also adjusted the window size order and obtained (v3.2-wo1) [32, 16, 8, 8, 16, 32], (v3.3-wo2) [8, 32, 64, 64, 32, 8] and (v3.4-wo3) [64, 64, 64, 64, 64, 64]. Based on the results in Table 2, we can conclude that all these variants are outperformed by our design and parameter selection.

Method ($\times 4$)	#Para. (K)	FLOPs (G)	PSNR (dB)	SSIM
v1.1-w/o C	0	0	-0.13	-0.0038
v1.2-w/o D	+188	+143.3	+0.05	+0.0010
v2.1-w/o HiE	-2	-0.3	-0.04	-0.0011
v2.2-w/o CSC	+46	+9.2	+0.02	+0.0002
v3.1-w/o U-Net	-29	-3.4	-0.06	-0.0011
v3.2-wo1	0	-0.7	-0.11	-0.0033
v3.3-wo2	0	0	-0.05	-0.0014
v3.4-wo3	0	+1.6	-0.03	-0.0012
(ours)	849	57.0	26.96	0.8104

Table 2. Ablation study results on the Urban100 [19] dataset. Here we report the PSNR/SSIM and complexity figure differences between each test variant and the original C2D-ISR model. All results are based on the $\times 4$ task and the SRFormer backbone only.

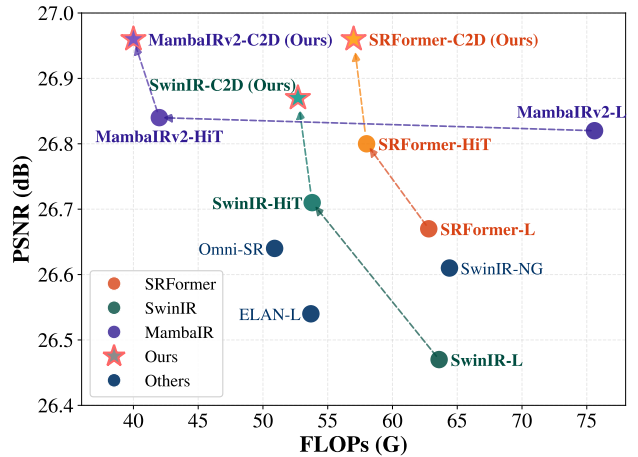


Figure 5. Complexity-performance trade-off visualization for selected ISR methods. The results are based on the Urban100 dataset and $\times 4$ task.

6. Conclusion

In this work, we present a novel optimization framework, C2D-ISR, designed to enhance lightweight attention-based ISR models. By leveraging continuous-scale pre-training, C2D-ISR enables the model to learn richer inter-scale correlations, leading to improved generalization and feature representation. To further boost SR performance, we designed a new Transformer architecture, HiET, which integrates hierarchical encoding mechanisms to capture multi-scale information more effectively than previous attention-based approaches. We have also employed a modified U-Net structure enabling adaptive window sizes at different levels, which achieves better multi-scale feature fusion with minimal additional computational overhead. By evaluating the proposed framework on three popular attention-based backbones, SwinIR-L, SRFormer-L, and MambaIRv2-L, we have confirmed the superior performance of our ap-

proach. C2D-ISR consistently outperforms the SOTA optimization framework, HiT, and the corresponding unoptimized lightweight SR models, with PSNR gains of up to 0.2dB (over HiT). Future work should focus on further improving computational efficiency, optimizing the efficiency of FFN, and extending the proposed framework to video super-resolution.

Acknowledgments

The authors appreciate the funding from Netflix Inc., the University of Bristol, and the UKRI MyWorld Strength in Places Programme (SIPF00006/1).

References

- [1] Mariana Afonso, Fan Zhang, and David R Bull. Video compression based on spatio-temporal resolution adaptation. *IEEE Transactions on Circuits and Systems for Video Technology*, 29(1):275–280, 2018. 2
- [2] Eirikur Agustsson and Radu Timofte. NTIRE 2017 challenge on single image super-resolution: Dataset and study. In *Proceedings of the IEEE conference on computer vision and pattern recognition workshops*, pages 126–135, 2017. 5
- [3] Namhyuk Ahn, Byungkon Kang, and Kyung-Ah Sohn. Fast, accurate, and lightweight super-resolution with cascading residual network. In *Proceedings of the European conference on computer vision (ECCV)*, pages 252–268, 2018. 2, 5
- [4] Marco Bevilacqua, Aline Roumy, Christine Guillemot, and Marie-Line Alberi Morel. Low-complexity single-image super-resolution based on nonnegative neighbor embedding. In *British Machine Vision Conference (BMVC)*, 2012. 6
- [5] Xiangyu Chen, Xintao Wang, Jiantao Zhou, Yu Qiao, and Chao Dong. Activating more pixels in image super-resolution transformer. In *Proceedings of the IEEE/CVF Conference on Computer Vision and Pattern Recognition (CVPR)*, pages 22367–22377, 2023. 2
- [6] Yinbo Chen, Sifei Liu, and Xiaolong Wang. Learning continuous image representation with local implicit image function. In *Proceedings of the IEEE/CVF conference on computer vision and pattern recognition*, pages 8628–8638, 2021. 2, 3, 5
- [7] Haram Choi, Jeongmin Lee, and Jihoon Yang. N-gram in swin transformers for efficient lightweight image super-resolution. In *Proceedings of the IEEE/CVF conference on computer vision and pattern recognition*, pages 2071–2081, 2023. 5
- [8] Marcos V Conde, Ui-Jin Choi, Maxime Burchi, and Radu Timofte. Swin2SR: Swin2 transformer for compressed image super-resolution and restoration. In *European Conference on Computer Vision*, pages 669–687. Springer, 2022. 2
- [9] Chao Dong, Chen Change Loy, Kaiming He, and Xiaoou Tang. Image super-resolution using deep convolutional networks. *IEEE transactions on pattern analysis and machine intelligence*, 38(2):295–307, 2015. 1, 2
- [10] Zongcai Du, Ding Liu, Jie Liu, Jie Tang, Gangshan Wu, and Lean Fu. Fast and memory-efficient network towards efficient image super-resolution. In *Proceedings of the IEEE/CVF Conference on Computer Vision and Pattern Recognition*, pages 853–862, 2022. 5
- [11] Hangxiang Fang, Xinyi Hu, and Haoji Hu. Cross knowledge distillation for image super-resolution. In *Proceedings of the 2022 6th International Conference on Video and Image Processing*, pages 162–168, 2022. 2
- [12] Jinsheng Fang, Hanjiang Lin, Xinyu Chen, and Kun Zeng. A hybrid network of cnn and transformer for lightweight image super-resolution. In *Proceedings of the IEEE/CVF conference on computer vision and pattern recognition*, pages 1103–1112, 2022. 3, 5
- [13] Mariana-Iuliana Georgescu, Radu Tudor Ionescu, Andreea-Iuliana Miron, Olivian Savencu, Nicolae-Cătălin Ristea, Nicolae Verga, and Fahad Shahbaz Khan. Multimodal multi-head convolutional attention with various kernel sizes for medical image super-resolution. In *Proceedings of the IEEE/CVF winter conference on applications of computer vision*, pages 2195–2205, 2023. 1
- [14] Jinjin Gu and Chao Dong. Interpreting super-resolution networks with local attribution maps. In *Proceedings of the IEEE/CVF Conference on Computer Vision and Pattern Recognition*, pages 9199–9208, 2021. 6, 8
- [15] Hang Guo, Yong Guo, Yaohua Zha, Yulun Zhang, Wenbo Li, Tao Dai, Shu-Tao Xia, and Yawei Li. Mambairv2: Attentive state space restoration. *arXiv preprint arXiv:2411.15269*, 2024. 2, 5, 6, 7
- [16] Hang Guo, Jinmin Li, Tao Dai, Zhihao Ouyang, Xudong Ren, and Shu-Tao Xia. Mambair: A simple baseline for image restoration with state-space model. In *ECCV*, 2024. 1, 2, 4
- [17] Zibin He, Tao Dai, Jian Lu, Yong Jiang, and Shu-Tao Xia. FAKD: Feature-affinity based knowledge distillation for efficient image super-resolution. In *2020 IEEE International Conference on Image Processing (ICIP)*, pages 518–522. IEEE, 2020. 2
- [18] Xuecai Hu, Haoyuan Mu, Xiangyu Zhang, Zilei Wang, Tieniu Tan, and Jian Sun. Meta-SR: A magnification-arbitrary network for super-resolution. In *Proceedings of the IEEE/CVF conference on computer vision and pattern recognition*, pages 1575–1584, 2019. 3
- [19] Jia-Bin Huang, Abhishek Singh, and Narendra Ahuja. Single image super-resolution from transformed self-exemplars. In *Proceedings of the IEEE conference on computer vision and pattern recognition*, pages 5197–5206, 2015. 6, 8
- [20] Zheng Hui, Xinbo Gao, Yunchu Yang, and Xiumei Wang. Lightweight image super-resolution with information multi-distillation network. In *Proceedings of the 27th acm international conference on multimedia*, pages 2024–2032, 2019. 5
- [21] Yuxuan Jiang, Jakub Nawala, Fan Zhang, and David Bull. Compressing deep image super-resolution models. In *2024 Picture Coding Symposium (PCS)*, pages 1–5. IEEE, 2024. 2
- [22] Yuxuan Jiang, Chen Feng, Fan Zhang, and David Bull. MTKD: Multi-teacher knowledge distillation for image

- super-resolution. In *ECCV*, pages 364–382. Springer, 2025. 2
- [23] Yuxuan Jiang, Ho Man Kwan, Tianhao Peng, Ge Gao, Fan Zhang, Xiaoqing Zhu, Joel Sole, and David Bull. Hiif: Hierarchical encoding based implicit image function for continuous super-resolution. *Proceedings of the IEEE/CVF Conference on Computer Vision and Pattern Recognition*, 2025. 2, 3, 4, 5
- [24] Jiwon Kim, Jung Kwon Lee, and Kyoung Mu Lee. Accurate image super-resolution using very deep convolutional networks. In *Proceedings of the IEEE conference on computer vision and pattern recognition*, pages 1646–1654, 2016. 1, 2
- [25] Jiwon Kim, Jung Kwon Lee, and Kyoung Mu Lee. Deeply-recursive convolutional network for image super-resolution. In *Proceedings of the IEEE conference on computer vision and pattern recognition*, pages 1637–1645, 2016. 2
- [26] Diederik P Kingma and Jimmy Ba. Adam: a method for stochastic optimization. *arXiv preprint arXiv:1412.6980*, 2014. 5
- [27] Ho Man Kwan, Ge Gao, Fan Zhang, Andrew Gower, and David Bull. HiNeRV: Video compression with hierarchical encoding based neural representation. In *NeurIPS*, 2023. 2, 3, 4
- [28] Ho Man Kwan, Ge Gao, Fan Zhang, Andrew Gower, and David Bull. NVRC: Neural video representation compression. *arXiv preprint arXiv:2409.07414*, 2024. 3
- [29] Wei-Sheng Lai, Jia-Bin Huang, Narendra Ahuja, and Ming-Hsuan Yang. Deep laplacian pyramid networks for fast and accurate super-resolution. In *Proceedings of the IEEE conference on computer vision and pattern recognition*, pages 624–632, 2017. 1
- [30] Jaewon Lee and Kyong Hwan Jin. Local texture estimator for implicit representation function. In *Proceedings of the IEEE/CVF conference on computer vision and pattern recognition*, pages 1929–1938, 2022. 2, 3
- [31] Jason Chun Lok Li, Steven Tin Sui Luo, Le Xu, and Ngai Wong. ASMR: activation-sharing multi-resolution coordinate networks for efficient inference. In *ICLR*. OpenReview.net, 2024. 2, 3
- [32] Yufei Li, Bruno Sixou, and Francois Peyrin. A review of the deep learning methods for medical images super resolution problems. *Irbm*, 42(2):120–133, 2021. 1
- [33] Jingyun Liang, Jiezhong Cao, Guolei Sun, Kai Zhang, Luc Van Gool, and Radu Timofte. SwinIR: Image restoration using swin transformer. In *Proceedings of the IEEE/CVF international conference on computer vision*, pages 1833–1844, 2021. 1, 2, 3, 4, 5, 6, 7
- [34] Jingyun Liang, Jiezhong Cao, Yuchen Fan, Kai Zhang, Rakesh Ranjan, Yawei Li, Radu Timofte, and Luc Van Gool. VRT: A video restoration transformer. *arXiv preprint arXiv:2201.12288*, 2022. 2
- [35] Bee Lim, Sanghyun Son, Heewon Kim, Seungjun Nah, and Kyoung Mu Lee. Enhanced deep residual networks for single image super-resolution. In *Proceedings of the IEEE conference on computer vision and pattern recognition workshops*, pages 136–144, 2017. 1, 2, 5
- [36] Jie Liu, Jie Tang, and Gangshan Wu. Residual feature distillation network for lightweight image super-resolution. In *Computer vision—ECCV 2020 workshops: Glasgow, UK, August 23–28, 2020, proceedings, part III 16*, pages 41–55. Springer, 2020. 5
- [37] Ilya Loshchilov and Frank Hutter. Sgdr: Stochastic gradient descent with warm restarts. *arXiv preprint arXiv:1608.03983*, 2016. 5
- [38] Zhisheng Lu, Juncheng Li, Hong Liu, Chaoyan Huang, Linlin Zhang, and Tiejiong Zeng. Transformer for single image super-resolution. In *Proceedings of the IEEE/CVF conference on computer vision and pattern recognition*, pages 457–466, 2022. 2, 3
- [39] Xiaotong Luo, Yuan Xie, Yulun Zhang, Yanyun Qu, Cuihua Li, and Yun Fu. LatticeNet: Towards lightweight image super-resolution with lattice block. In *Computer Vision—ECCV 2020: 16th European Conference, Glasgow, UK, August 23–28, 2020, Proceedings, Part XXII 16*, pages 272–289. Springer, 2020. 2, 5
- [40] David Martin, Charless Fowlkes, Doron Tal, and Jitendra Malik. A database of human segmented natural images and its application to evaluating segmentation algorithms and measuring ecological statistics. In *Proceedings Eighth IEEE International Conference on Computer Vision. ICCV 2001*, pages 416–423. IEEE, 2001. 6
- [41] Yusuke Matsui, Kota Ito, Yuji Aramaki, Azuma Fujimoto, Toru Ogawa, Toshihiko Yamasaki, and Kiyoharu Aizawa. Sketch-based manga retrieval using manga109 dataset. *Multimedia tools and applications*, 76:21811–21838, 2017. 6
- [42] Karam Park, Jae Woong Soh, and Nam Ik Cho. Efficient attention-sharing information distillation transformer for lightweight single image super-resolution. *arXiv preprint arXiv:2501.15774*, 2025. 3
- [43] Adam Paszke, Sam Gross, Francisco Massa, Adam Lerer, James Bradbury, Gregory Chanan, Trevor Killeen, Zeming Lin, Natalia Gimelshein, Luca Antiga, et al. Pytorch: An imperative style, high-performance deep learning library. *Advances in neural information processing systems*, 32, 2019. 5
- [44] Yulin Ren, Xin Li, Mengxi Guo, Bingchen Li, Shijie Zhao, and Zhibo Chen. MambaCSR: Dual-interleaved scanning for compressed image super-resolution with ssms, 2024. 2
- [45] Olaf Ronneberger, Philipp Fischer, and Thomas Brox. U-net: Convolutional networks for biomedical image segmentation. In *Medical image computing and computer-assisted intervention—MICCAI 2015: 18th international conference, Munich, Germany, October 5-9, 2015, proceedings, part III 18*, pages 234–241. Springer, 2015. 2
- [46] Yuan Shi, Bin Xia, Xiaoyu Jin, Xing Wang, Tianyu Zhao, Xin Xia, Xuefeng Xiao, and Wenming Yang. VmambaIR: Visual state space model for image restoration. *arXiv preprint arXiv:2403.11423*, 2024. 2
- [47] Ying Tai, Jian Yang, and Xiaoming Liu. Image super-resolution via deep recursive residual network. In *Proceedings of the IEEE conference on computer vision and pattern recognition*, pages 3147–3155, 2017. 2
- [48] Ying Tai, Jian Yang, Xiaoming Liu, and Chunyan Xu. Memnet: A persistent memory network for image restoration. In *Proceedings of the IEEE international conference on computer vision*, pages 4539–4547, 2017. 2

- [49] Radu Timofte, Eirikur Agustsson, Luc Van Gool, Ming-Hsuan Yang, and Lei Zhang. NTIRE 2017 challenge on single image super-resolution: Methods and results. In *Proceedings of the IEEE conference on computer vision and pattern recognition workshops*, pages 114–125, 2017. 5
- [50] Hang Wang, Xuanhong Chen, Bingbing Ni, Yutian Liu, and Jinfan Liu. Omni aggregation networks for lightweight image super-resolution. In *Proceedings of the IEEE/CVF Conference on Computer Vision and Pattern Recognition*, pages 22378–22387, 2023. 3, 5
- [51] Huan Wang, Yulun Zhang, Can Qin, Luc Van Gool, and Yun Fu. Global aligned structured sparsity learning for efficient image super-resolution. *IEEE transactions on pattern analysis and machine intelligence*, 45(9):10974–10989, 2023. 5
- [52] Peijuan Wang, Bulent Bayram, and Elif Sertel. A comprehensive review on deep learning based remote sensing image super-resolution methods. *Earth-Science Reviews*, 232: 104110, 2022. 2
- [53] Zhou Wang, Alan C Bovik, Hamid R Sheikh, and Eero P Simoncelli. Image Quality Assessment: from error visibility to structural similarity. *IEEE transactions on image processing*, 13(4):600–612, 2004. 6
- [54] Zhihao Wang, Jian Chen, and Steven CH Hoi. Deep learning for image super-resolution: A survey. *IEEE transactions on pattern analysis and machine intelligence*, 43(10):3365–3387, 2020. 2
- [55] Zhendong Wang, Xiaodong Cun, Jianmin Bao, Wengang Zhou, Jianzhuang Liu, and Houqiang Li. Uformer: A general u-shaped transformer for image restoration. In *Proceedings of the IEEE/CVF conference on computer vision and pattern recognition*, pages 17683–17693, 2022. 2
- [56] Yi Xiao, Xin Su, Qiangqiang Yuan, Denghong Liu, Huanfeng Shen, and Liangpei Zhang. Satellite video super-resolution via multiscale deformable convolution alignment and temporal grouping projection. *IEEE Transactions on Geoscience and Remote Sensing*, 60:1–19, 2021. 2
- [57] Lei Yu, Xinpeng Li, Youwei Li, Ting Jiang, Qi Wu, Haoqiang Fan, and Shuaicheng Liu. Dipnet: Efficiency distillation and iterative pruning for image super-resolution. In *Proceedings of the IEEE/CVF Conference on Computer Vision and Pattern Recognition*, pages 1692–1701, 2023. 2
- [58] Roman Zeyde, Michael Elad, and Matan Protter. On single image scale-up using sparse-representations. In *Curves and Surfaces: 7th International Conference, Avignon, France, June 24-30, 2010, Revised Selected Papers 7*, pages 711–730. Springer, 2012. 6
- [59] Fan Zhang, Mariana Afonso, and David R Bull. ViSTRA2: Video coding using spatial resolution and effective bit depth adaptation. *Signal Processing: Image Communication*, 97: 116355, 2021. 2
- [60] Liangpei Zhang, Hongyan Zhang, Huanfeng Shen, and Pingxiang Li. A super-resolution reconstruction algorithm for surveillance images. *Signal Processing*, 90(3):848–859, 2010. 2
- [61] Xindong Zhang, Hui Zeng, Shi Guo, and Lei Zhang. Efficient long-range attention network for image super-resolution. In *European conference on computer vision*, pages 649–667. Springer, 2022. 3, 4, 5
- [62] Xiang Zhang, Yulun Zhang, and Fisher Yu. Hit-sr: Hierarchical transformer for efficient image super-resolution. In *European Conference on Computer Vision*, pages 483–500. Springer, 2024. 2, 3, 4, 5, 6, 7, 8
- [63] Yulun Zhang, Kunpeng Li, Kai Li, Lichen Wang, Bineng Zhong, and Yun Fu. Image super-resolution using very deep residual channel attention networks. In *Proceedings of the European conference on computer vision (ECCV)*, pages 286–301, 2018. 2
- [64] Yulun Zhang, Huan Wang, Can Qin, and Yun Fu. Learning efficient image super-resolution networks via structure-regularized pruning. In *International conference on learning representations*, 2021. 2
- [65] Yupeng Zhou, Zhen Li, Chun-Le Guo, Song Bai, Ming-Ming Cheng, and Qibin Hou. Srformer: Permuted self-attention for single image super-resolution. In *Proceedings of the IEEE/CVF International Conference on Computer Vision*, pages 12780–12791, 2023. 2, 4, 5, 6, 7, 8
- [66] Qiang Zhu, Pengfei Li, and Qianhui Li. Attention retractable frequency fusion transformer for image super resolution. In *Proceedings of the IEEE/CVF Conference on Computer Vision and Pattern Recognition*, pages 1756–1763, 2023. 2